Supplementary Figure 1. Aberrant *GREM1* expression and phenotype of HMPS lesions.

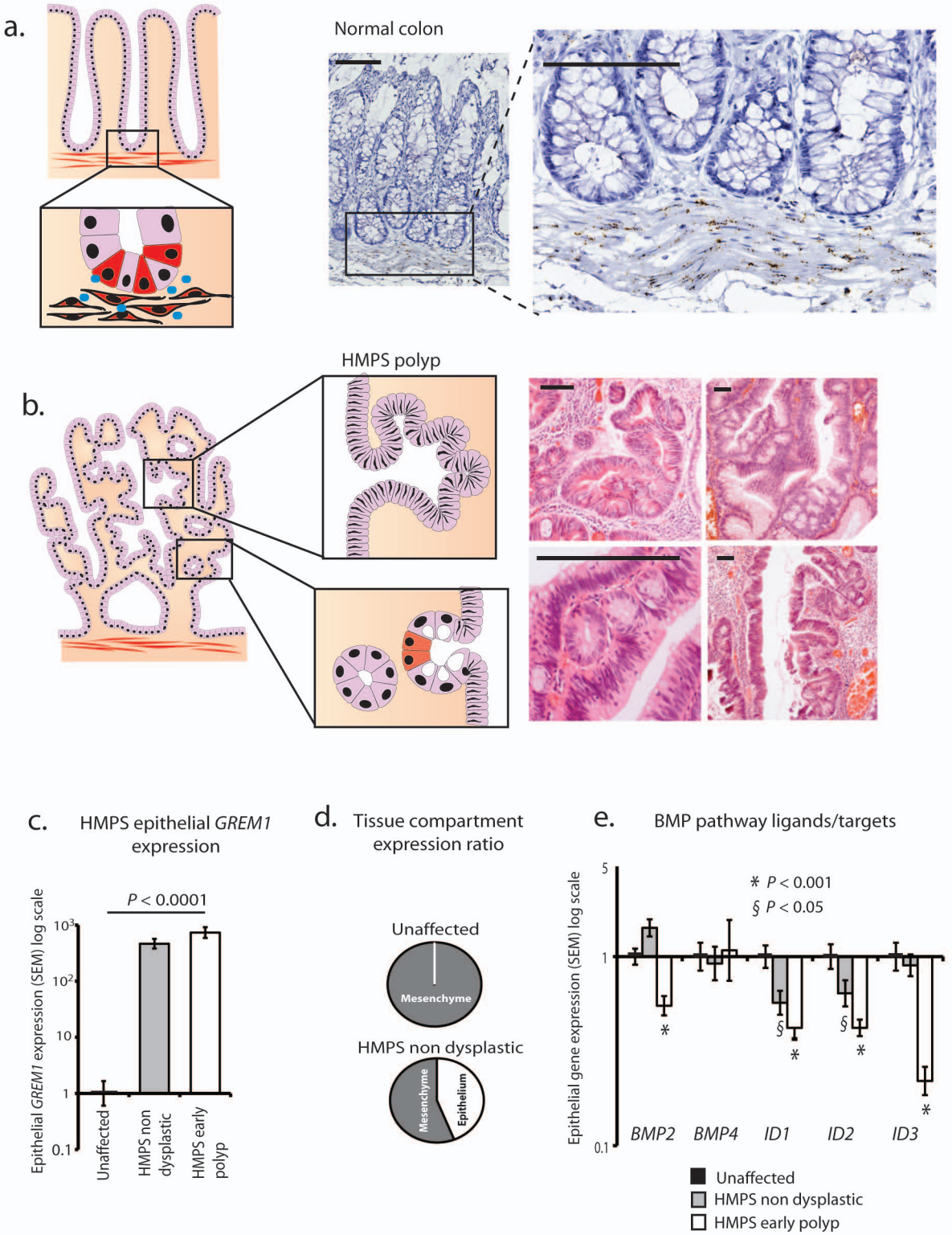


**(a)** Left panel: diagrammatic representation of physiological *GREM1* expression (blue dots) confined to the sub-cryptal myofibroblasts with the secreted protein acting on the cells of the crypt base (including crypt base columnar cells – red cells). Right panel: Human *GREM1 in situ* hybridisation showing restricted expression (brown dots) from the sub-cryptal myofibroblast cells. **(b)** Left panel: Diagrammatic example of HMPS polyp morphology. Right panel: Ectopic crypts can have dysplastic pencillate like nuclear appearance or can appear non-dysplastic and goblet cell rich with complex clusters of ectopic crypts in advanced polyps. **(c)** Profound aberrant epithelial expression of *GREM1* in HMPS non-dysplastic and early polyp tissue with no candidate gene somatic mutation. **(d)** Change in tissue compartment expression ratio in HMPS patients based on ratio of qRT-PCR ddCt measurements. **(e)** BMP ligand and target expression in HMPS patients. Scale bars are 100 μm.

Supplementary Figure 2. Human tissue somatic mutation.

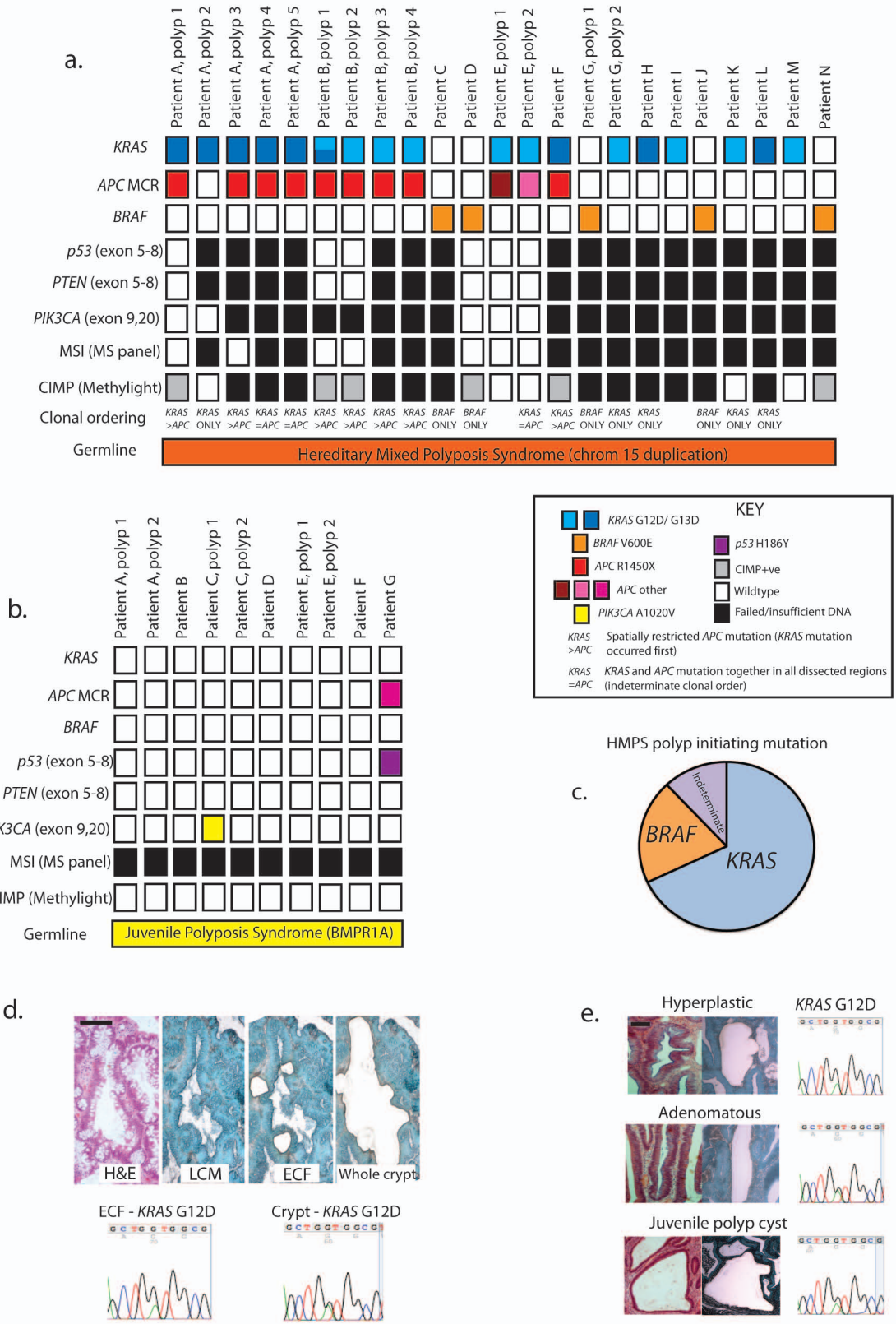


**(a)** HMPS polyps. **(b)** Juvenile Polyposis Syndrome polyps. Each column represents the results of candidate gene sequencing of a single dissected polyp. Clonal ordering row shows polyps that underwent individual crypt or multi-regional dissection to allow spatially distinct mutation identification **(c)** HMPS polyp initiating mutations determined by clonal ordering analysis. In 2 polyps, selective sweep of both *KRAS* and *APC* mutation across every dissected region meant that the initiating mutation could not be determined (indeterminate). **(d)** Microdissection of individual ectopic crypts showed that these contained the same mutation as the crypt body. **(e)** Different HMPS crypt morphological subtypes. had the same initiating mutation in each histological crypt type. Scale bars are 100 μm.

Supplementary Figure 3. *Vill-Grem1* mouse generation and BMP pathway expression changes.

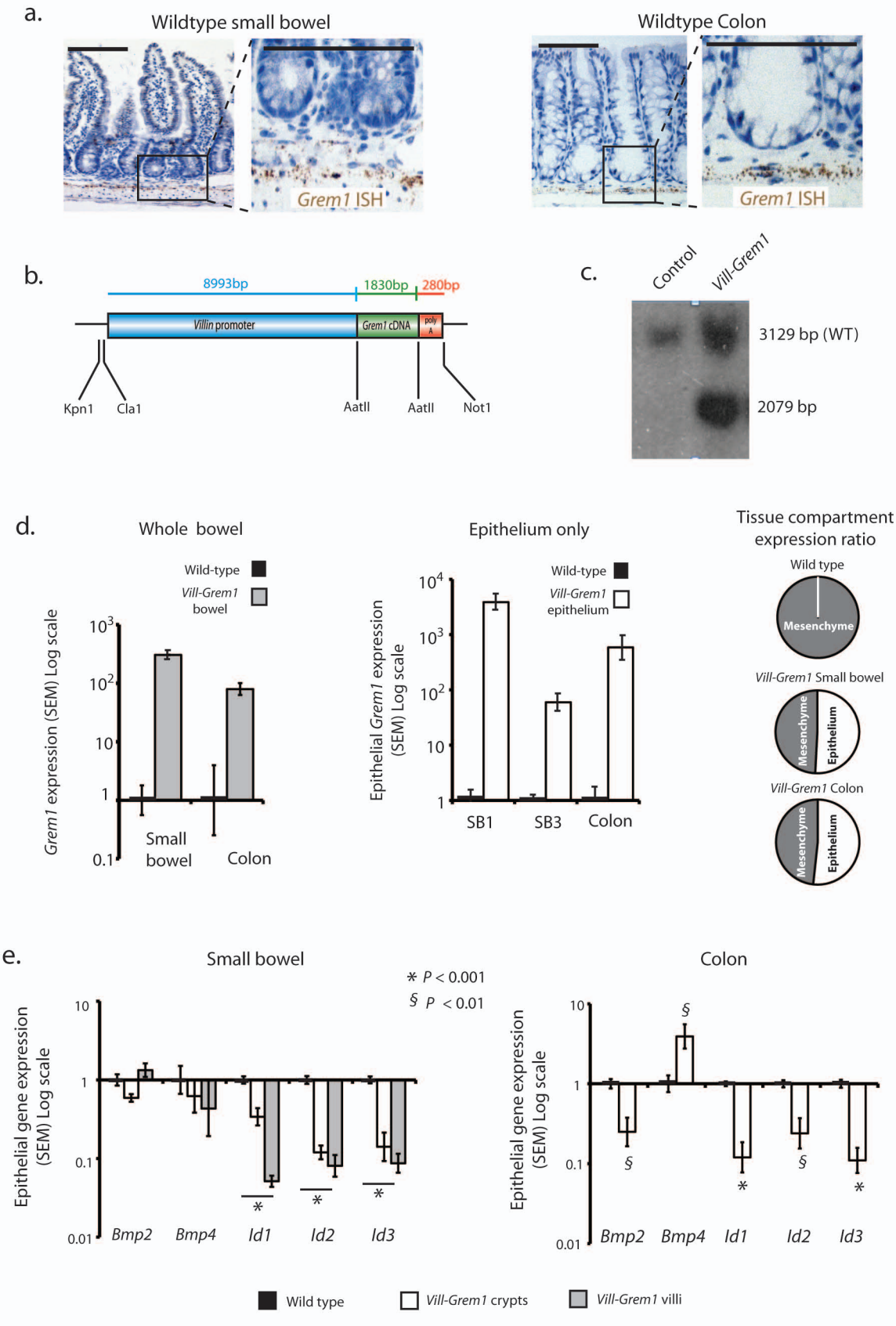


**(a)** Wildtype mouse *Grem1 in situ* hybridisation showing restricted physiological expression of *Grem1* **(b)** *Vill-Grem1* mouse construct map. *Grem1* cDNA was inserted into the *Villin-MES-SV40polyA* plasmid downstream of the 9Kb villin promoter using *AatII* sites. **(c)** Southern blot of founder line mouse tail DNA showed a 2079 bp fragment of the inserted transgene. **(d)** *Grem1* expression in *Vill-Grem1* mice versus wild-type littermate. Left panel, whole small bowel and colon ($P < 0.001$, t test n = 4). Middle panel: epithelium alone along the cephalic-caudal axis of the intestine ($P < 0.001$, t-test, n = 12). Right panel: The tissue compartment expression ratio (based on ratio of qRT-PCR ddCt measurements) in wild-type and *Vill-Grem1* mice shows that the increased epithelial contribution accounts for the increase in overall intestinal expression of *Grem1*. **(e)** BMP pathway constituent expression in *Vill-Grem1*and control mice. Scale bars are 100 μm.

Supplementary Figure 4. *Vill-Grem1* mouse phenotype

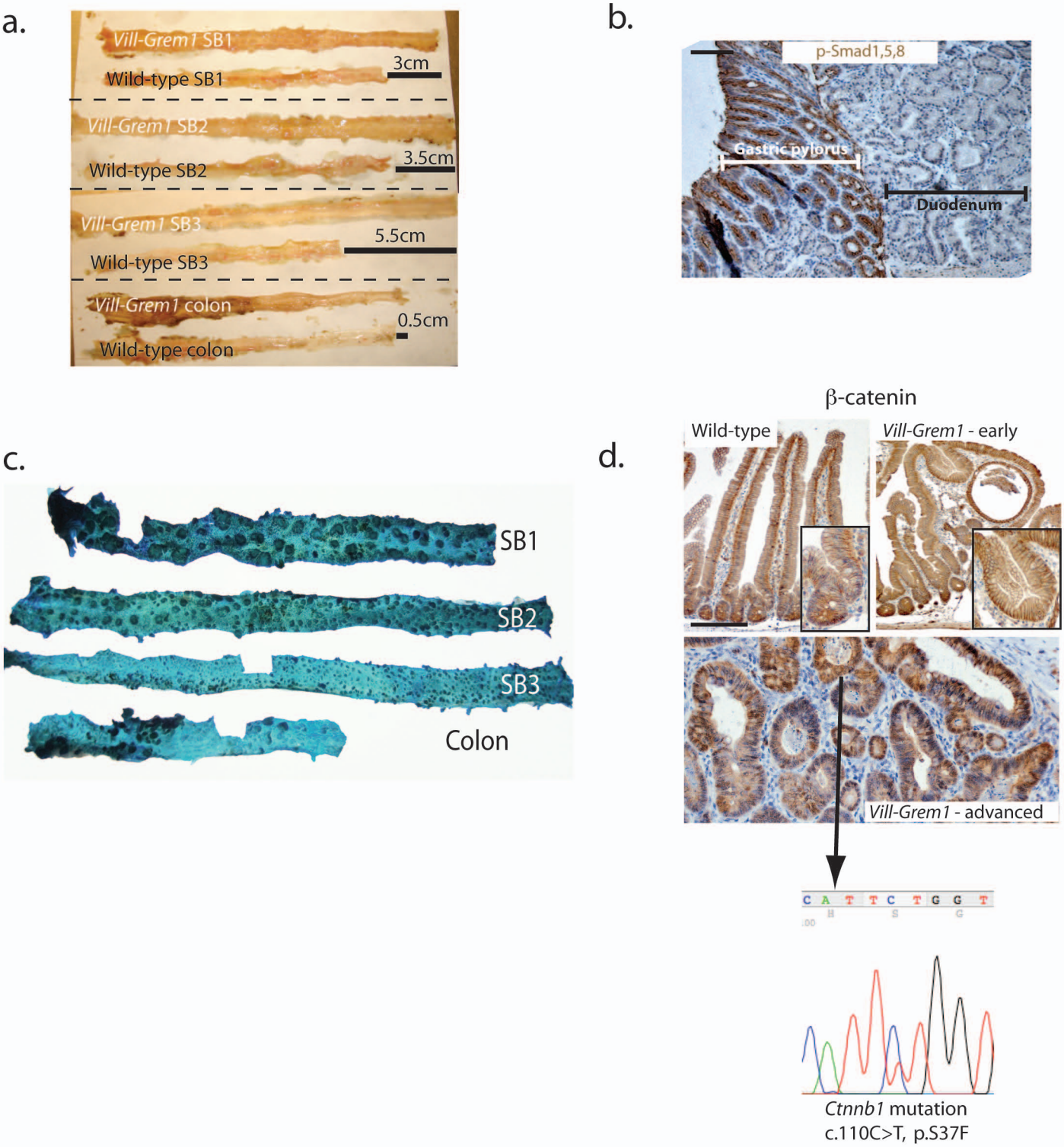


**(a)** *Vill-Grem1* intestinal size. Side-by-side dissection of a six-month old *Vill-Grem1* mouse intestine and a wild-type littermate. **(b)** p-Smad1,5,8 staining of gastroduodenal junction of *Vill-Grem1* mouse**.** p-Smad1,5,8, staining used as a marker of epithelial BMP activity. Sharp demarcation of p-Smad1,5,8 activity was seen between the positive gastric epithelium and the negative duodenal epithelium. **(c)** Macroscopic appearance of seven-month old *Vill-Grem1* mouse intestine. Stained with methylene blue to highlight discrete polyps seen in each intestinal segment. **(d)** Membranous β-catenin stain in unaffected mucosa and early *Vill-Grem1* mouse polyps. In some more advanced lesions, foci of cytoplasmic and nuclear staining could be seen. Sequencing of these areas revealed an activating *Ctnnb1* mutation in three different lesions. SB1 – small bowel 1, SB2 – small bowel 2, SB3 – small bowel 3. Scale bars are 100 μm (unless stated).

Supplementary figure 5. Effect of *Grem1* manipulation on conventional tumourigenesis

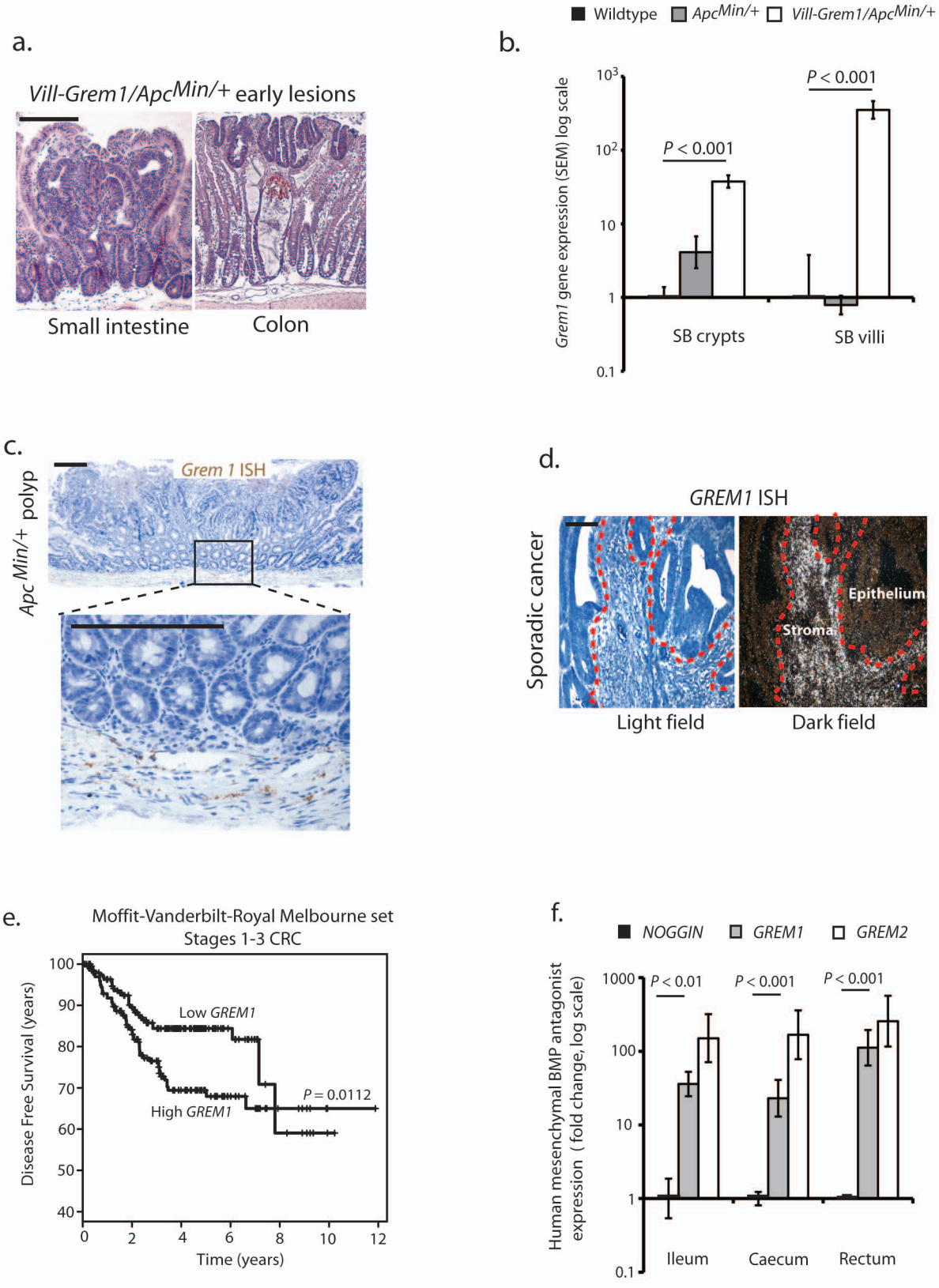


**(a)** Early *Vill-Grem1/Apc*$^{Min/+}$ small intestinal polyps rapidly develop intravillus crypt dysplasia often encompassed by non-dysplastic serrated epithelium. In the colon dysplastic aberrant crypt foci start at the luminal surface and bud downwards into the mucosa. **(b)** Epithelial *Grem1* expression in *Apc*$^{Min/+}$ *and Vill-Grem1/Apc*$^{Min/+}$ *mice* ($P < 0.001$, t test, n = 3). **(c)** *In situ* hybridisation in *Apc*$^{Min}$ mouse polyp shows predominantly mesenchymal expression of *Grem1*. **(d)** *GREM1 in situ* hybridisation in human sporadic CRC reveals profound upregulation of *GREM1* expression in the desmoplastic stroma of a sporadic tumour. **(e)** Effect of *GREM1* expression on CRC survival in the Moffit-Vanderbilt-Royal Melbourne set ($P = 0.0112$, log rank test). **(f)** Physiological expression of BMP antagonists in the normal human mesenchyme showing less physiological expression of *Noggin* in the human intestinal mesenchyme in comparison to *GREM1* and *GREM2*. ($P < 0.01$, t-test, n = 4). Scale bars are 100 μm.

Supplementary Figure 6. *Grem1* knockout mice

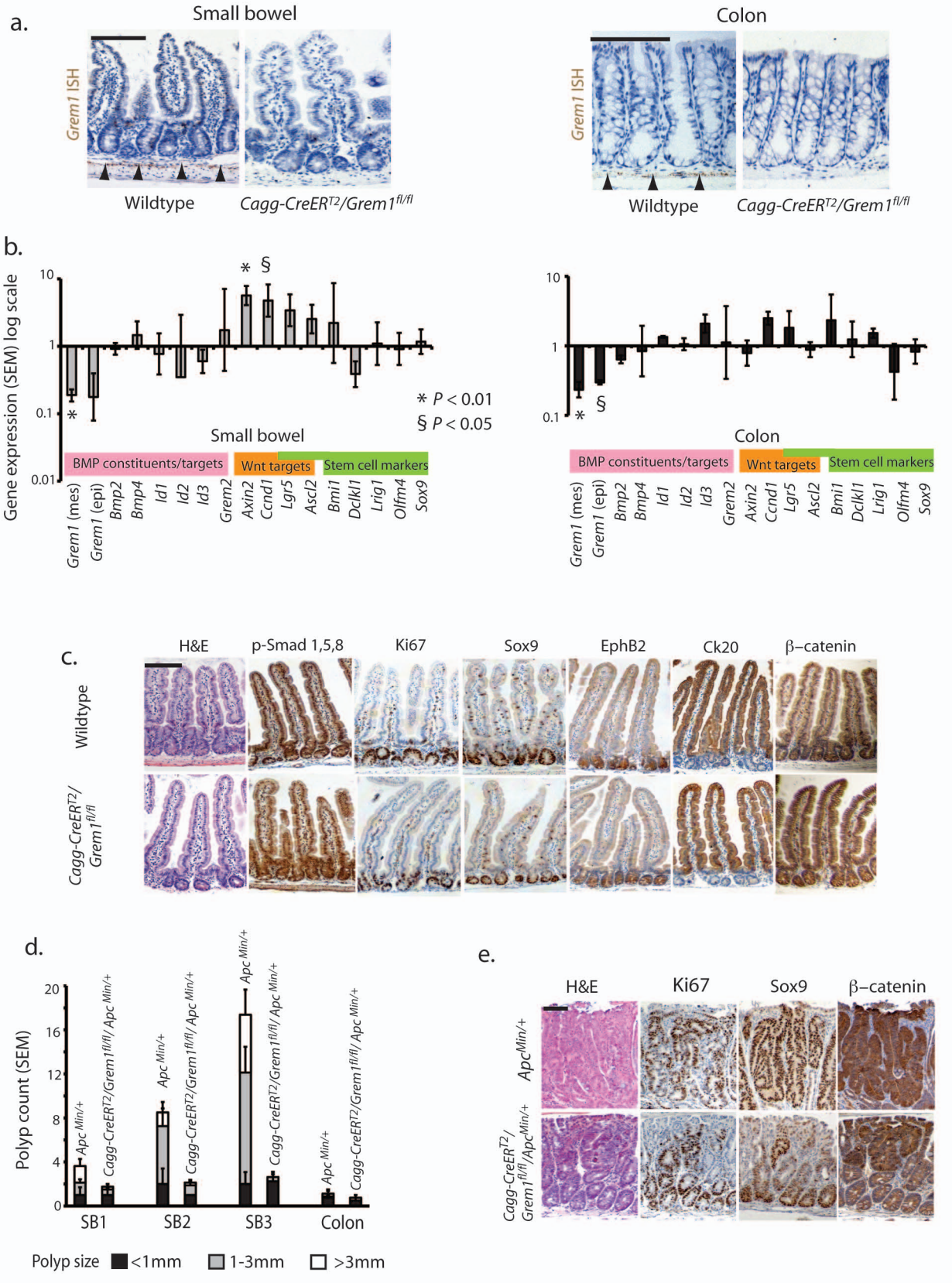


**(a)** *Grem1 in situ* hybridisation showing effective knockout of the normal expression of *Grem1* in *Cagg-CreER$^{T2}$/Grem1$^{fl/fl}$* mice. Normal expression in control mice denoted by black arrowheads. **(b)** qRT-PCR of selected genes in the epithelium of *Cagg-CreER$^{T2}$/Grem1$^{fl/fl}$* versus wildtype mice. **(c)** Immunohistochemical analysis of *Cagg-CreER$^{T2}$/Grem1$^{fl/fl}$* small intestine. No significant difference to wildtype could be detected (n = 3 mice). **(d)** Difference in polyp size in mean 248 day old *Apc$^{Min/+}$* and age matched *Cagg-CreER$^{T2}$/Grem1$^{fl/fl}$/Apc$^{Min/+}$* mice. ($P < 0.001$, logistic regression (n = 4 mice for test and non injected control). **(e)** Immunohistochemical comparison of *Apc$^{Min/+}$* and *Cagg-CreER$^{T2}$/Grem1$^{fl/fl}$/Apc$^{Min/+}$* polyps (n = 4 mice). Scale bars are 100 μm.

Supplementary Figure 7. Traditional serrated adenomas

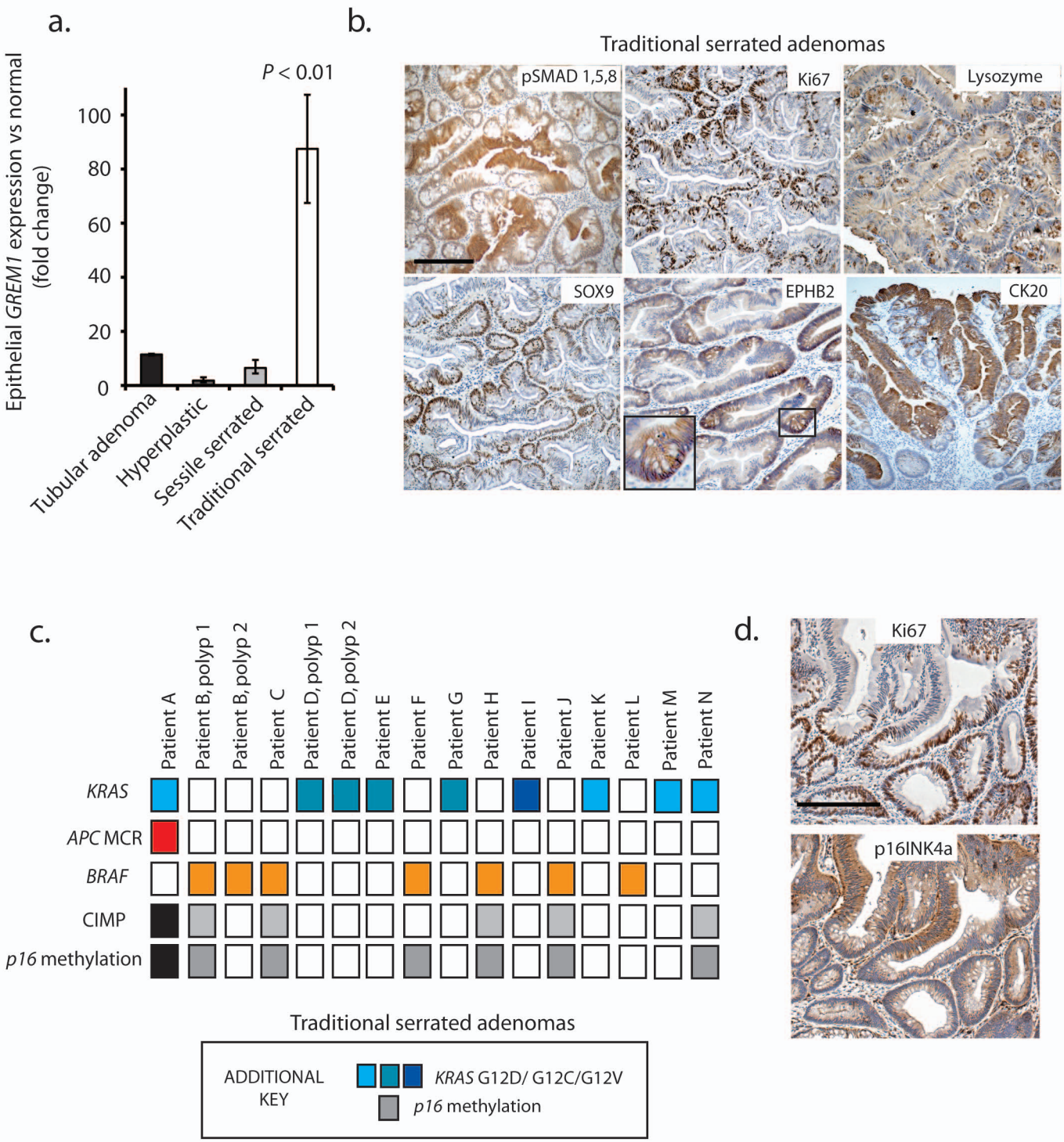


**(a)** Epithelial *GREM1* expression in different human polyp subtypes. with increased epithelial expression in traditional serrated adenomas ($P < 0.01$, t-test, n = 4). **(b)** TSAs shared a similar immunohistochemical molecular phenotype to HMPS polyps (n = 10 polyps). **(c)** TSA somatic mutations. Each column represents the results of candidate gene sequencing/methylation analysis of a single dissected polyp. **(d)** Loss of p16INK4a immunostaining in TSA lesions correlated with cell proliferation detected by Ki67 stain. Scale bars are 100 μm.